Drastic Sensing Enhancement Using Acoustic Bubbles For Surface-Based Microfluidic Sensors

A. De Vellis[a,1], D. Gritsenko[a,1], Y. Lin[a], Z. Wu[b], X. Zhang[c], Y. Pan[a], W. Xue[d], J. Xu[a,*]

[a] *Department of Mechanical and Industrial Engineering, University of Illinois, Chicago, IL 60607,USA.*

[b] *School of Science, Beijing University of Posts and Telecommunications,Beijing 100876, China.*

[c] *Department of Mechanical Engineering, Columbia University, New York, NY 10027,USA.*

[d] *Department of Mechanical Engineering, College of Engineering, Rowan University, Glassboro, NJ 08028,USA.*

Abstract

There is a high demand for ultrafast biosensors for industrial and public health applications. However, the performance of existing sensors is often limited by the slow mass transport process in traditional pressure-driven microfluidic devices. In this paper we show for the first time, that acoustic microbubbles trapped in prefabricated cavities in a micro-chamber are capable of enhancing fluid sample mixing that results in faster delivery of target species to the sensor surface. We demonstrate a drastic reduction of sensor response time (up to 21.3 fold) for surface-based nanosenors in presence of resonantly actuated microbubbles. The obtained results are valid in a wide pH (4-10) range and agree well with previous studies.

Keywords: sensing enhancement, microstreaming, microfluidics, resonant frequency

*Corresponding author

Email address: jiexu@uic.edu (J. Xu)

[1]These authors contributed equally to this work.

1. Introduction

Effective mass transport has been a major challenge in fluids engineering at the microscale. For example, mixing has been considered as "the most fundamental and difficult-to-achieve issue" in microfluidics [1]. On the other hand, mass transport has also gradually become a major roadblock in the biosensors community. Nowadays, there is a high demand for ultrasensitive and cost effective sensors in many pressing situations,varying from biodefense and cancer marker detection [2, 3, 4] to environmental monitoring [5] and food safety control [6]. Since the sensor signal-to-noise ratio increases with decreasing sensor size, many researchers are expending considerable effort to fabricate smaller devices [7]. Despite all these efforts, the performance of current affinity-based sensors seems to have hit a wall around femtomolar resolution. Researchers have started to realize that, in most cases, the question is no longer whether the sensor would respond to the molecule; it is actually whether and how fast the molecule could reach the sensor [8, 9]. Indeed, it will take more than a day for the first molecule (in case of a 20-based ssDNA) to find a 10 nm sized sensor at 1 fM concentration via diffusion only [8]. Therefore, convection is often used to help with analyte delivery. However, in traditional pressure-driven microfluidic devices, molecules are delivered in one direction, and most of them flow in the middle of the channel without reaching the sensor due to the no-slip boundary condition. It inhibits the analyte replenishment rate near a sensor and thus physically limits its performance. Unfortunately, increasing the flow rate will only drastically increase the pressure in the channel up to the device breakage point. Therefore, there is a critical need to explore methods that can actively and effectively transport molecules to sensors without causing a global increase in pressure.

A variety of microfluidic mixing devices have been extensively developed in the last two decades. They can generally be classified as passive and active mixers, both of which have attracted considerable attention in the microfluidic community. Comprehensive reviews of different mixing mechanisms were given by Nguyen [10] and Capretto [11]. Passive micromixers usually rely on specific geometry designs to cause secondary flows inside a laminar pressure-driven flow. Passive mixers (such as herringbone grooves [12]) often require long channel length and rely upon high flow rates, and thus high pressure drops. Active micromixers, in contrast, employ external energy to introduce a local turmoil in a liquid to enhance mixing, thus providing better and more

controllable mixing without global increase in pressure.

As a unique actuation scheme, microscale oscillating bubbles in an acoustic field often exhibit bizarre phenomena such as a strong force field near the bubbles (called the secondary radiation force or Bjerknes force) [13] and locally-confined microflow (called microstreaming) [14, 15]. If controlled well, these phenomena can be surprisingly useful for flow control and object manipulation in a microchannels [16, 17, 18] and microchambers [19]. For example, oscillating microbubbles can be used as microfluidic pumps [20], micro tweezers [21, 22, 23] and micro filters [24]. In this paper we demonstrate that significant sensing enhancement for graphene-based nanosensors can be achieved once the diffusion limits were overcome. The reduction of sensor response time was mainly attributed to microstreaming generated by resonantly actuated microbubbles. In addition, it was shown that the reduction of sensor response time exhibited resonant behavior with resonant peak when plotted with respect to frequency. The working range of the frequency is therefore determined from this peak for sensor operation.

2. Material and methods

2.1. Chemicals

Buffer solutions (Fisher Scientific Buffer solutions) with pH in range from 4 to 10 were used. Water solution of microspheres (DUKE Standards) of various diameters (1, 5 and 10 μm) were applied for flow visualization. The 3D printing was supplied with Formlabs resin (Clear Resin). Polydimethylsiloxane (PDMS) was fabricated using conventional technique. Silicone elastomer base and curing agent from SYLGARD were mixed in proportion 10:1 and cured for 20 minutes.

2.2. Sensing cell

A micromilling machine (Minitech Mini-Mill/3) was used to fabricate microcavity arrays (cavity diameter 75 μm) on four PMMA plates, and a desktop 3D printer (Formlabs 1+) was used to fabricate a fixture box. Specifically, two sizes of plates $1 \times 4.6 \times 13.7$ mm^3 and $1 \times 7.4 \times 13.7$ mm^3 were used to make respectively, with 200 μm center-to-center distance and 150 μm depth. These plates were then fixed vertically inside the fixture box separated by 1 mm gap and placed above the sensor. A four-plate geometry was chosen due to the ease of fabrication via milling. Resin polymeric material provided the deformability of the box[25], necessary to insert the plates and fix them

securely. The liquid was injected into the box through circular opening (d = 2 mm) in a top wall using a syringe (Monoject 1 mL Insulin Syringe, Permanent Needle, 28 G $\times$ 1/2″). The sensing cell was placed in a Petri dish (Steve Spangler Science) secured with PDMS all around. The scheme of the sensing cell and complete scheme of experimental setup are given at Fig. 1.

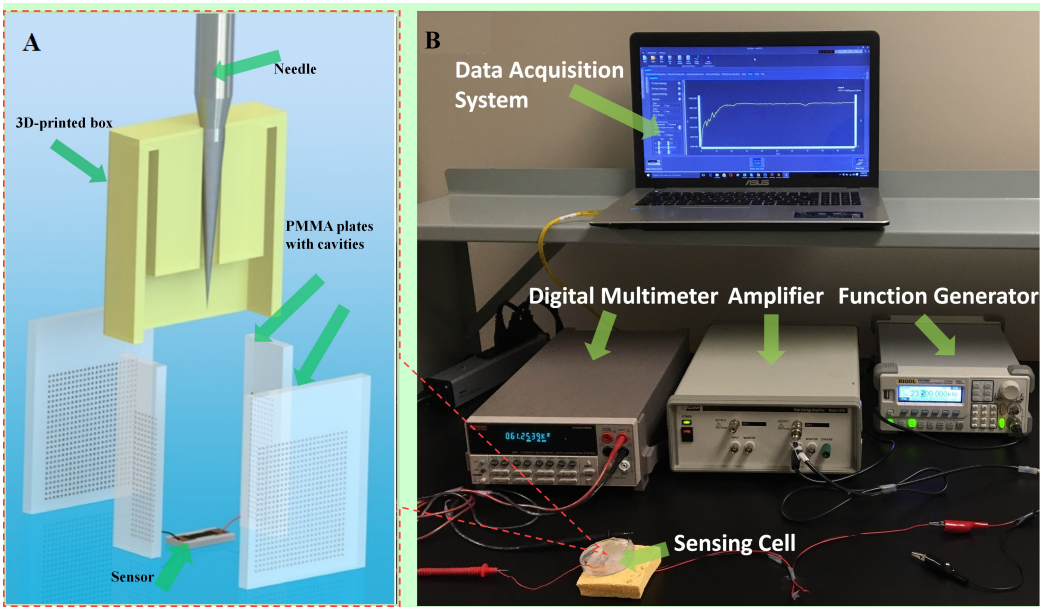

Figure 1: A) PMMA plates with microcavities were fixed vertically inside a 3D-printed box and placed above a graphene nanosensor. pH buffers were injected into the box from the top and microbubbles were trapped passively inside the cavities. B) Experimental setup. Function generator provided square wave (20V p-p) and amplified with High Voltage Amplifier to 120V p-p. Output signal was recorded with Digital Multimeter.

2.3. Actuation

The microbubbles generated on prefabricated cavities were actuated as follows. A RIGOL function generator (DG1022A Arbitrary Waveform Function Generator) provided square wave (20 V peak-to-peak) which was amplified with a high voltage power amplifier (Krohn-Hite 7602(M) Wideband Power Amplifier) up to 120 V peak-to-peak. An amplified signal was applied to a disc piezo transducer (APC International, d=20 mm, t=2 mm, f_r=99 kHz). The transducer was fixed on the bottom side of Petri dish with insulating transparent tape and positioned just below sensing cell.

2.4. Working frequency

Before performing sensing experiments, we need to estimate the working frequency of the bubbles. However, the classical Minnaert frequency is only applicable for a free-standing spherical bubble [26]. For bubbles trapped in a cavity, it is extremely difficult to develop a theory for calculating their resonant frequencies, although some recent attempts were done for square shaped cavities[27]. On the other hand, extensive experimental characterization of microbubbles can be found in literature. For instance, second order dependence for voltage vs streaming speed was demonstrated in [28] and bubble oscillation amplitude was visualized and quantified in [13]. Thus, we determine the working frequency of the bubbles experimentally in this paper. To do so, we placed the PMMA-containing box on top of a transparent glass slide, so that the microstreaming can be observed (traced by 1, 5, 10 μm polystyrene particles) through the glass slide using an inverted microscope (Nikon Eclipse Ti-S). A piezo transducer was placed on the edge of the glass slide (as close as possible to box). The frequency was adjusted in a range from 1 kHz to 100 kHz with 100 Hz steps. For most of the frequency values no streaming was observed and particles moved simply due to diffusion with a very low speed. The particle velocity increased remarkably when approaching the working range and it appeared to maximize $f = 23.5$ kHz that was chosen as a working frequency.

2.5. Readout

The resistance of graphene was monitored with Keithley multimeter (2701 Digital Multi-Meter). It provided readout accuracy of 0.1Ω. Data acquisition was performed with KickStart software (KickStart Instrument Control Software). A sampling rate of 250/s was used. Data analysis was accomplished using OriginPro software (OriginPro 2015).

2.6. Sensor structure and operating principles

The graphene was grown on a copper substrate via chemical vapor deposition (CVD) and then transferred to SiO_2. As reported previously [29, 30, 31, 32] this transfer introduces additional p-doping in graphene. When placing the buffer solution on graphene surface, it creates an electrochemical double layer which is "impermeable" for charged ions, in particular for hydroxonium/H_3O^+ and hydroxyl/OH^- ions. This double layer acts as a parallel plate capacitor. An accumulation of ions on the double layer attracts charges with opposite

signs on the counter layer thus modifying the resistance of the sensor, in this case, graphene [33].

3. Results and discussion

3.1. Sensor Calibration

The sensor was first calibrated *i.e.* the resistance saturation value for each pH buffer was determined. Previous studies showed an increasing trend for the resistance up to a saturation value (shape similar to a monotonic crescent function with horizontal asymptote). Tests were made without the microbubbles actuation. The linear decreasing trend for resistance with increasing pH was demonstrated that agreed with Lei *et al.* [33]. The fitting equation was:

$$R = -2508 \times \mathrm{pH} + 46405 \tag{1}$$

with $r^2 = 0.98$. Fitting results are given at Fig. 2A. The resistance was measured at 10 μA direct current. This dependence can be explained as follows. In acidic buffers, H_3O^+ ions dominate; they accumulate on the double layer and cannot go directly into the graphene. Instead of the addition p-doping, the accumulated H_3O^+ ions repel holes in graphene, resulting in a lower p-doping effect. For base buffers, OH^- ions accumulate on the double layer and attract more holes in graphene. This causes a p-doping effect. Since graphene on SiO_2 is p-doping, acidic buffers reduce p-doping and cause a higher resistance; base buffers increase p-doping and cause a lower resistance. Fig. 2B demonstrated how saturation was reached.

3.2. Sensor response time reduction

Drastic reduction of sensing times was observed for the case of resonant bubble actuation. Table 1 summarized reduction achieved for various pH values. The best possible time reduction was achieved for pH=4. Fig. 3 compared diffusion-induced and actuated-bubbles-induced cases. Fig. 3A clearly demonstrates sensing time reduction from 780 s to 35 s for pH=4. Similar trend was observed for other pH values (Fig. 3B,C).

The results in Table 1 show sensor response time for pH from 4-10, and the time reduction η was determined as:

$$\eta = \frac{T_{without} - T_{with}}{T_{with}}, \tag{2}$$

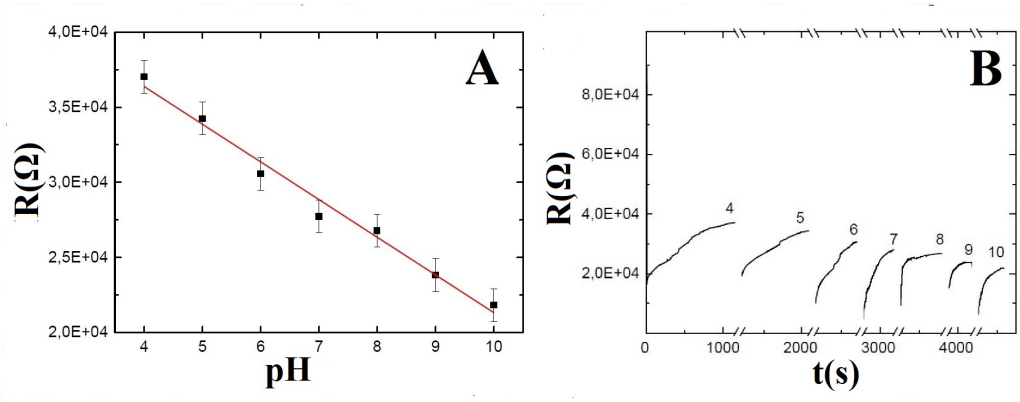

Figure 2: Sensor calibration A)Resistance saturation pH dependence. B)Resistance saturation time dependence (the numbers on the graphs represent pH values)

Table 1: Sensor response time **T** with and without bubbles actuation for every pH value tested.

pH	**T** w/o bubbles(s)	**T** w/ bubbles (s)	Sensor response time reduction η (fold)
4	780	35	21.30
5	760	45	15.90
6	740	35	20.15
7	475	35	12.60
8	490	50	8.80
9	270	70	2.85
10	460	55	7.35

here T_{with} and $T_{without}$ stand for sensor response time with and without bubble actuation respectively. From this table, we can see that without bubble actuation, sensing times are longer in acid, and with bubble actuation, sensing times are longer in alkali, which indicates that diffusion limits were indeed overcome by bubble actuation. The following explanation can be adopted. The sensor response time has two contributing factors: mass transfer and adsorption, or $T = T_{\text{mass transfer}} + T_{\text{adsorption}}$. Without actuation, the sensing process is limited by mass transfer ($T_{\text{mass transfer}} \gg T_{\text{adsorption}}$); since H_3O^+ ions are larger compared to OH^- ions and have lower mobility the sensing time is higher for H_3O^+ ions, *i.e.*, in acid buffer. When the bubbles are actuated, adsorption becomes the limiting step ($T_{\text{mass transfer}} \ll T_{\text{adsorption}}$). It is likely that H_3O^+ ions have higher adsorption rate compared to hydroxyl

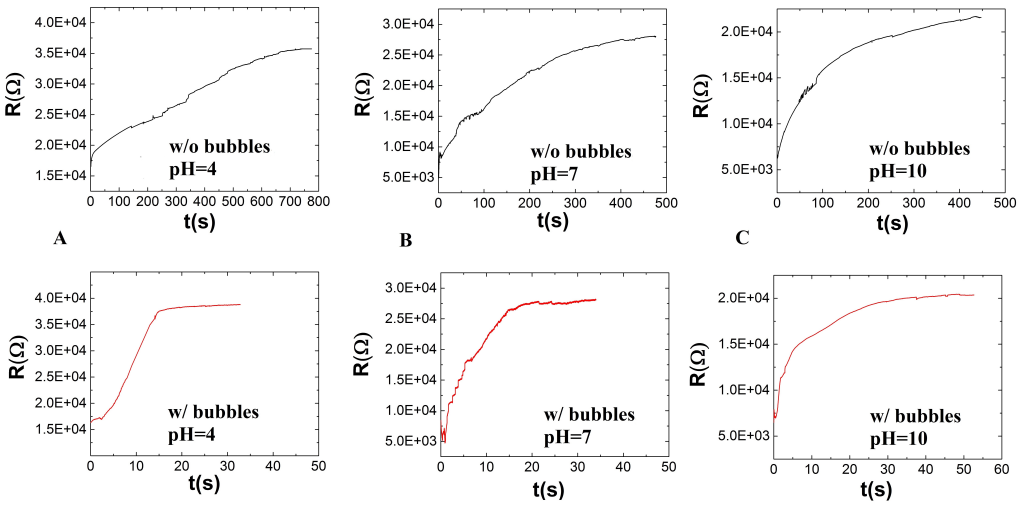

Figure 3: Sensor response times for A) pH=4 B) pH=7 C) pH=10: top row, Resistance as a function of time w/o bubbles actuation; bottom row, Resistance as a function of time with bubbles actuation.

ions due to the ease of ion rearrangement on graphene [34], and therefore the sensor response time is shorter in acid.

3.3. Operation optimization

Driving voltage was one of the parameters that required optimization. The voltage range of 30-150 V was tested.Sensor response time reduction was demonstrated as the voltage increased(Fig.4 A). However, as 120 V was achieved no further reduction was observed. In order to avoid significant heating of piezo transducer that may introduce additional undesirable noises to the system, an operating voltage of 120 V has been chosen.

Additionally, we also studied the changes in sensor response time as the piezo actuator was detuned from the working frequency (23.5 kHz) and with varying voltages. The buffer with pH=4 was used for these tests. It was shown that sensor response time reduction improves with increasing driving voltage (up to 4 times) (Figure 4A) and sensor response time reduction η exhibited resonant behavior (Figure 4B) with a resonant peak (Quality factor Q=11). Thus, the operating frequency range for this sensing cell was determined (Δf=2.2 kHz).

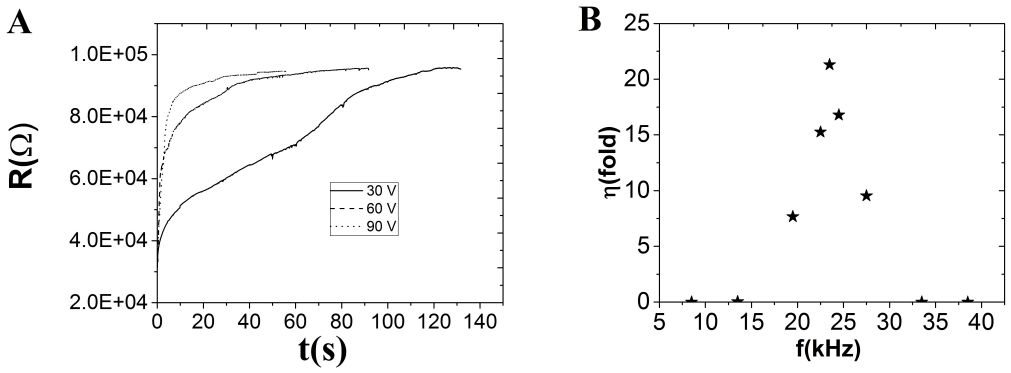

Figure 4: Operation optimization A) Resistance time dependence for various driving voltages. B)Working frequency range for pH=4.

4. Conclusions

We have demonstrated the possibility to overcome the diffusion limits and reduce the sensor response time with actuated air-liquid bubbles trapped on prefabricated cavities. We suppose that the reduction in the sensor response time was caused by the enhanced mass transport near the sensor due to the microstreaming phenomenon. Finally, sensing enhancement was demonstrated for wide pH range (4-10). The best performance of the sensor was achieved for pH=4 (21.3 fold).

The proposed prototype can be useful for biochemical applications such as detection of large target molecules including glucose, DNA, cancer markers and proteins.

This research was supported by J. Xu's start up fund at UIC.

[1] Y. K. Suh, S. Kang, A review on mixing in microfluidics, Micromachines 1 (3) (2010) 82–111.

[2] M. Tsutsui, S. Rahong, Y. Iizumi, T. Okazaki, M. Taniguchi, T. Kawai, Single-molecule sensing electrode embedded in-plane nanopore, Sci. Rep. 1 (2011) 1–6.

[3] A. M. Armani, R. P. Kulkarni, S. E. Fraser, R. C. Flagan, K. J. Vahala, Label-free, single-molecule detection with optical microcavities, Science 317 (5839) (2007) 783–787.

[4] Z. Zhang, J. Xu, B. Hong, X. Chen, The effects of 3D channel geometry on CTC passing pressure–towards deformability-based cancer cell separation, Lab Chip 14 (14) (2014) 2576–2584.

[5] Y. Lin, D. Gritsenko, S. Feng, Y. C. Teh, X. Lu, J. Xu, Detection of heavy metal by paper-based microfluidics, Biosens. Bioelectron. 83 (2016) 256–266.

[6] L. Guo, J. Feng, Z. Fang, J. Xu, X. Lu, Application of microfluidic "lab-on-a-chip" for the detection of mycotoxins in foods, Trends. Food. Sci. Technol. 46 (2) (2015) 252–263.

[7] S. A. Solovitz, J. Zhao, W. Xue, J. Xu, Uniform flow control for a multipassage microfluidic sensor, J. Fluids Eng. 135 (2) (2013) 021101.

[8] P. E. Sheehan, L. J. Whitman, Detection limits for nanoscale biosensors, Nano Lett. 5 (4) (2005) 803–807.

[9] T. M. Squires, R. J. Messinger, S. R. Manalis, Making it stick: convection, reaction and diffusion in surface-based biosensors, Nat. Biotechnol. 26 (4) (2008) 417–426.

[10] N.-T. Nguyen, Z. Wu, Micromixers—a review, J. Micromech. Microeng. 15 (2) (2004) R1.

[11] L. Capretto, W. Cheng, M. Hill, X. Zhang, Micromixing within microfluidic devices, in: Microfluidics, Springer, 27–68, 2011.

[12] A. D. Stroock, S. K. Dertinger, A. Ajdari, I. Mezić, H. A. Stone, G. M. Whitesides, Chaotic mixer for microchannels, Science 295 (5555) (2002) 647–651.

[13] Y. Chen, Z. Fang, B. Merritt, D. Strack, J. Xu, S. Lee, Onset of particle trapping and release via acoustic bubbles, Lab Chip (2016) 3024–3032.

[14] A. Hashmi, G. Heiman, G. Yu, M. Lewis, H.-J. Kwon, J. Xu, Oscillating bubbles in teardrop cavities for microflow control, Microfluid. Nanofluidics 14 (3-4) (2013) 591–596.

[15] D. Ahmed, X. Mao, J. Shi, B. K. Juluri, T. J. Huang, A millisecond micromixer via single-bubble-based acoustic streaming, Lab Chip 9 (18) (2009) 2738–2741.

[16] A. Hashmi, G. Yu, M. Reilly-Collette, G. Heiman, J. Xu, Oscillating bubbles: a versatile tool for lab on a chip applications, Lab Chip 12 (21) (2012) 4216–4227.

[17] Y. Xu, A. Hashmi, G. Yu, X. Lu, H.-J. Kwon, X. Chen, J. Xu, Microbubble array for on-chip worm processing, Appl. Phys. Lett. 102 (2) (2013) 023702.

[18] D. Ahmed, A. Ozcelik, N. Bojanala, N. Nama, A. Upadhyay, Y. Chen, W. Hanna-Rose, T. J. Huang, Rotational manipulation of single cells and organisms using acoustic waves, Nat. Commun. 7 (2016) 11085.

[19] Y. Xie, N. Nama, P. Li, Z. Mao, P.-H. Huang, C. Zhao, F. Costanzo, T. J. Huang, Probing Cell Deformability via Acoustically Actuated Bubbles, Small (2015) 902–910.

[20] A. R. Tovar, M. V. Patel, A. P. Lee, Lateral air cavities for microfluidic pumping with the use of acoustic energy, Microfluid. Nanofluidics 10 (6) (2011) 1269–1278.

[21] S. K. Chung, S. K. Cho, On-chip manipulation of objects using mobile oscillating bubbles, J. Micromech. Microeng. 18 (12) (2008) 125024.

[22] S. K. Chung, S. K. Cho, 3-D manipulation of millimeter-and micro-sized objects using an acoustically excited oscillating bubble, Microfluid. Nanofluidics 6 (2) (2009) 261–265.

[23] J. Kwon, J. Yang, S. Lee, K. Rhee, S. Chung, Electromagnetically actuated micromanipulator using an acoustically oscillating bubble, J. Micromech. Microeng. 21 (11) (2011) 115023.

[24] P. Rogers, A. Neild, Selective particle trapping using an oscillating microbubble, Lab Chip 11 (21) (2011) 3710–3715.

[25] A. A. Yazdi, A. Popma, W. Wong, T. Nguyen, Y. Pan, J. Xu, 3D printing: an emerging tool for novel microfluidics and lab-on-a-chip applications, Microfluid. Nanofluidics 20 (3) (2016) 1–18.

[26] C. E. Brennen, Cavitation and bubble dynamics, Cambridge University Press, 2013.

[27] C. Chindam, N. Nama, M. I. Lapsley, F. Costanzo, T. J. Huang, Theory and experiment on resonant frequencies of liquid-air interfaces trapped in microfluidic devices, J. Appl. Phys. 114 (19) (2013) 194503.

[28] J. Xu, D. Attinger, Control and ultrasonic actuation of a gas–liquid interface in a microfluidic chip, J. Micromech. Microeng. 17 (3) (2007) 609.

[29] B. Mailly-Giacchetti, A. Hsu, H. Wang, V. Vinciguerra, F. Pappalardo, L. Occhipinti, E. Guidetti, S. Coffa, J. Kong, T. Palacios, pH sensing properties of graphene solution-gated field-effect transistors, J. Appl. Phys. 114 (8) (2013) 084505.

[30] L. H. Hess, M. V. Hauf, M. Seifert, F. Speck, T. Seyller, M. Stutzmann, I. D. Sharp, J. A. Garrido, High-transconductance graphene solution-gated field effect transistors, Appl. Phys. Lett. 99 (3) (2011) 033503.

[31] J. Bai, L. Liao, H. Zhou, R. Cheng, L. Liu, Y. Huang, X. Duan, Top-gated chemical vapor deposition grown graphene transistors with current saturation, Nano Lett. 11 (6) (2011) 2555–2559.

[32] T. O. Wehling, A. I. Lichtenstein, M. I. Katsnelson, First-principles studies of water adsorption on graphene: The role of the substrate, Appl. Phys. Lett. 93 (20) (2008) 202110.

[33] N. Lei, P. Li, W. Xue, J. Xu, Simple graphene chemiresistors as pH sensors: fabrication and characterization, Meas. Sci. Technol. 22 (10) (2011) 107002.

[34] T. M. Squires, S. R. Quake, Microfluidics: Fluid physics at the nanoliter scale, Rev. Mod. Phys. 77 (3) (2005) 977.

Fig.1. A) PMMA plates with microcavities were fixed vertically inside a 3D-printed box and placed above a graphene nanosensor. pH buffers were injected into the box from the top and microbubbles were trapped passively inside the cavities. B) Experimental setup. Function generator provided square wave (20V p-p) and amplified with High Voltage Amplifier to 120V p-p. Output signal was recorded with Digital Multimeter.

Fig.2. Sensor calibration A)Resistance saturation pH dependence. B)Resistance saturation time dependence(the numbers on the graphs represent pH values).

Fig.3. Sensor response times for A) pH=4 B) pH=7 C) pH=10:top row, Resistance as a function of time w/o bubbles actuation; bottom row, Resistance as a function of time with bubbles' actuation.

Fig.4. Operation optimization A) Resistance time dependence for various driving voltages. B)Working frequency range for pH=4.